PAPER

Check for updates

Preparation and characterization of 3D hydroxyapatite/collagen scaffolds and its application in bone regeneration with bone morphogenetic protein-2

Hongyu Xie,†[a] Sijie Ruan,†[b] Minlong Zhao,[c] Jindong Long,[a] Xueling Ma,[a] Jinhong Guo[d] and Xuandong Lin ⬤ *[a]

Desirable bone engineering materials should have a conducive three-dimensional (3D) structure and bioactive mediators for guided bone regeneration. In the present study, hydroxyapatite (HA)/collagen (Col) scaffolds were prepared by an optimized freeze-drying process. The porosity, moisture content, and mechanical properties of the composite have been investigated. The micro-morphology and structure were analyzed with scanning electron microscopy (SEM) and transmission electron microscopy (TEM), confirmed that self-cross-linked HA/Col was evenly distributed and formed a 3D porous scaffold. The physicochemical/mechanical characterization was carried out by Fourier transform infrared spectroscopy (FT-IR) and X-ray diffraction (XRD). Morphological observation and CCK-8 assay of co-culture cells indicated that HA/Col scaffolds were biocompatible. Then HA/Col scaffolds coupled with recombinant human bone morphogenetic proteins 2 (rhBMP-2) were implanted in the mandibular critical size defect in rats, and histological staining was used to evaluate the bone reconstruction. The result showed that HA/Col coupled with rhBMP-2 could significantly improve the formation of new bone and angiogenesis within the scaffolds as well as the proliferation and differentiation of osteoblasts. Thanks to the encouraging osteogenesis effects, the well-defined 3D scaffolds (HA/Col) cooperating with bioactive agents (rhBMP-2) are expected to be a promising candidate for bone tissue engineering applied to regenerative medicine.

1. Introduction

Severe maxillofacial bone damage that requires tissue reconstruction may be connected with congenital disabilities, osteoradionecrosis, tumors, or trauma, and traditionally, these debilitating causes were addressed by bone grafting procedures.[1,2] Nevertheless, the repair of bone abnormalities is still a challenge since autograft harvesting has clinical drawbacks and limitations, while allografts have inferior ossification and a high risk of immunological rejection.[3–6] Consequently, since the 1980s, various types of artificial bone substitutes have been developed.[7,8]

As a complex inorganic–organic composite material, natural bone is made up of well-organized hydroxyapatite nanocrystals ($Ca_{10}(PO_4)_6(OH)_2$, HA) and collagen fiber (Col). Collagen serves as a perfect basis for biomaterials considering their ready availability, nontoxicity, and native structure. The architecture and biochemical characteristics of collagens have been widely studied, and the latest literature reported that there were 28 collagen subtypes have been identified.[9–11] Nevertheless, the most remembered is type I collagen, the leading organic constituents of bone, tendon, and tooth. Consequently, collagen is regarded as one of the most beneficial natural biomaterials. In the biomedical field, collagen can be processed in scaffolding material, promoting cell migration, wound healing, and tissue regeneration.

HA has been widely used as an artificial bone substitute and took a great deal of attention for hard tissue applications considering its bioactive, osteoconductive, and biodegradable properties.[12–14] However, due to its severe brittleness insufficient fracture toughness, fatigue breakage, and brittle damage, the use of pure HA is rather constrained.[15]

Thus, composite materials obtained from HA and polymer, such as collagen, are highly recommended in bone tissue

[a] *College of Stomatology, Hospital of Stomatology, Guangxi Medical University, No. 10 Shuangyong Road, Nanning, Guangxi, 530021, PR China. E-mail: xuandonglingxmu@163.com; Tel: +86-15777128619*

[b] *Department of Anesthesiology, Central Hospital of Shaoyang, Shaoyang, Hunan, 422000, China*

[c] *Department of Implantology, Anyang Sixth People's Hospital, Anyang, Henan, 455000, China*

[d] *Guangxi Medical University, Nanning, Guangxi, 530021, China*

† These authors contributed equally to this work.

reconstruction. Recently, a loose and porous HA/Col was developed, which owning sponge-like flexibility as well as superb handling properties. Thanks to the porous HA/Col's structural characteristics, cells can easily transfer into the "porous sponge," thus improving osteoconduction and remodeling at the implant site.[16]

Growth factors have been used as comprehensive tools for the induction of bone formation and regeneration. Bone morphogenetic proteins (BMPs) are growth factors that effectively design bone formation in humans by recapitulating the different stages of bone development.[17] Among them, BMP-2 is the most intensely studied BMP in osteogenesis and has been demonstrated to promote bone formation, especially some commercialized rhBMP-2 that are coated with soy lecithin and gelatin would be helpful for creating sustained-release medical systems.[18–20]

Even though there are currently some relevant studies on HA/Col scaffolds impregnated with recombinant human bone morphogenetic proteins 2 (rhBMP-2) or spatially-controlled delivery of rhBMP-2 from HA scaffolds coated with collagen I film for bone regeneration, either of them lacking the chemical characterization and exploration between them, or the comprehensive and cell experiments *in vitro*.[21,22]

In the present work, we assembled a 3D-type composite scaffold from different ratios of Col and nano-HA by optimized blending and freeze-drying methods, then the properties of HA/Col were characterized and assessed for choosing the most suitable materials for bioremediation. To further improve their ability to induce bone formation and regeneration, the HA/Col was further with the rhBMP-2 with slow release during application. By using the porous HA/Col with rhBMP-2, good effect of bone defect healing was demonstrated.

2. Materials and methods

2.1. Materials

Type I atelocollagen (2.9–3.2 mg mL^{-1}, purity > 99.9%) was obtained from the company of Advanced BioMatrix (Carlsbad, US). Hydroxyapatite (nanopowder, <200 nm particle size) was supplied by the company of Sigma-Aldrich (Poznan, Poland). For the *in vitro* study, α-Minimum Essential Medium (Invitrogen, Carlsbad, USA), fetal bovine serum (FBS; Invitrogen), cell counting kit-8 (CCK-8; GLPBIO, Montclair, CA, US) were applied. The rhBMP-2 was purchased from Jiuyuan Gene Engineering Co., Ltd (Zhejiang, China).

2.2. Preparation and characterization of HA/Col

2.2.1. Preparation of HA/Col. One part of chilled 10× PBS (0.1 mol L^{-1}) was slowly added to 8 parts of chilled collagen solution (3.0 mg mL^{-1}) with gentle swirling. Adjust pH of the mixture to 7.3–7.7 using sterile 0.1 M NaOH with monitor pH adjustment. Then the final volume was adjusted to a total of 10 parts with sterile water. Warm to 37 °C for 90–120 min, the 3-D Gel of collagen took shape. Then, the nanopowder of HA was transferred to the 3-D collagen Gel. The experimental materials for the final HA/Col composites were mixed, and the concentration and amount of the starting substances were set for HA/Col weight ratio to be 60/20, 80/20, and 100/20. After sufficient magnetic stirring for two hours, the HA/Col mixtures were moved to a polystyrene container and then set in a freezer at −22 °C. The wholly frozen composites were freeze-dried at −60 °C and 100 Pa for 48 h.

2.2.2. Porosity measurement. The porosity of the prepared HA/Col (60/20, 80/20, and 100/20) and Col scaffolds was measured by liquid displacement method.[23] Each of the scaffolds was immersed in absolute ethanol for 5 min, and the porosity was calculated using the following formula:

$$\text{Porosity} = (V_1 - V_2)/(V_2 - V_3) \times 100\%$$

where, V_1 = the volume of absolute ethanol, V_2 = the total volume of the thoroughly impregnated scaffold into ethanol, V_3 = residual volume of ethanol.

All measurements were repeated four times ($n = 4$).

2.2.3. *In vitro* swelling study. Different scaffolds were cut into regular cubes (20 mm × 20 mm × 20 mm) and immersed in phosphate-buffered saline (PBS) for two hours (pH 7.4, 37 °C). The swelling (DS) was calculated using this formula:

$$\text{DS} = (W_1 - W_2)/W_2 \times 100\%$$

where W_1 and W_2 were the wet and dry weights of the scaffolds. The moisture retention capacity and DS at predetermined timepoints were determined when transferred in a desiccator at 25 °C for 18 h.[24]

2.2.4. Mechanical test. The Microcomputer Controlled Electronic Universal Testing Machine (WDW-20E, Jinan Hengsisheng Instrument Equipment Co., Ltd, Shandong, China) was used to measure the tensile strength (TS) and percentage of elongation at break (Eb) of 3D scaffolds. The load capacity was set to 100 N with a crosshead speed of 40 mm min^{-1}. 3D scaffolds were clipped into regular shape with 100 mm long and 20 mm wide. TS (MPa) and Eb were computed by the following formulas:

$$\text{TS} = \text{load}/(\text{width} \times \text{thickness}) \text{ MPa}$$

$$\text{Eb} = (\text{displacement at break})/(\text{sample length}) \times 100\%$$

2.2.5. Biodegradability study. The 3D scaffolds were soaked in PBS with lysozyme (10 000 U mL^{-1}) at 37 °C for up to 3 weeks. At a certain point, the 3D scaffolds were cleaned with sterile deionized water to get rid of ions attached to the surface. Then the samples were lyophilized consecutively. The degradation of 3D scaffolds was computed by the following formulas:

$$\text{Biodegradability} = (W_1 - W_t)/W_1 \times 100\%$$

where W_1 is the initial and W_t is the dry weight of 3D scaffolds at different points in time.

2.2.6. Stability test. The freeze-dried 3D scaffolds were immersed in 2 solutions with different pH (4 and 7) at room temperature. The vacuum was used to dry the scaffolds for 48 h

at 50 °C. The weight loss of 3D scaffolds was conducted by a second weighing to confirm its stabilities. The stability of the 3D scaffolds was calculated with the following equation:

$$S = (W_2/W_1) \times 100\%$$

where W_1 and W_2 are the weights of dried 3D scaffolds before and after the test.

2.2.7. Scanning electron microscopy (SEM) analysis. After the freeze-drying, the morphology of collagen sponges modified with 80 wt% of HA was investigated using Scanning Electron Microscopy (SEM; Hitachi SU8010, Tokyo, Japan). Samples were examined at an accelerating voltage of 15–20 kV.

2.2.8. Fourier transform infrared spectroscopy (FT-IR) analysis. The chemical reaction between HA nanocrystals and functional groups of collagens was evaluated by Fourier transform infrared spectroscopy (FT-IR; PerkinElmer Spectrum Two, US) within the scanning range of 4000 to 650 cm^{-1} using a KBr pellet technique.

2.2.9. X-ray diffraction (XRD). The crystalline phase of HA nanocrystals and collagen scaffold were analyzed via X-ray diffraction (XRD) (Smartlab9, Rigaku Corporation, D_{max} = 1400, 40 kV, 110 mA). The data were collected in the 2θ range of 10–80° at a scan rate of 0.02° min^{-1}.

2.2.10. Transmission electron microscope (TEM) analysis. To observe the hierarchical relationship between nano-HA and collagen scaffold at a microscopic level, the transmission electron microscope (TEM; Hitachi H-7650, Tokyo, Japan) at an acceleration voltage of 100 kV to observe the morphology. All images of TEM were negatively stained with 2% (w/v) uranyl acetate.

2.3. Biocompatibility in vitro

2.3.1. Cell culture. Human dental pulp cells were used for this study. Dental pulp tissues were acquired from viable tissues of clinically healthy dental pulp from human adult premolars and third molars for orthodontic treatment. Before the sample collection, all patients gave written informed consent before participating in this study. The ethics committee of Guangxi Medical University approved the experimental protocols. The α-Minimum Essential Medium was used to culture dental pulp cells (DPCs), which was supplemented with 10% fetal bovine serum and 1% antibiotics. The culture system was kept in a humidified atmosphere of 95% air and 5% CO$_2$.

2.3.2. Morphological observation. DPCs were seeded into a 24-well microtiter plate with a density of 3×10^4 cells per well. The cell culture system was incubated for 24 h at 37 °C and 5% CO$_2$ to allow adhesion. Subsequently, the DPCs were treated with different concentrations (25%, 50%, 75%, and 100%) of leach liquor for HA/Col. The concentration of 100% leach liquor was set as 0.2 g mL^{-1} and the extracting time was 72 h, the main component of which was α-Minimum Essential Medium with 10% fetal bovine serum, then incubated for 12 h, 24 h, and 48 h. The medium only and phenol (0.64%) with the medium were set to the control group. Finally, the cellular morphological changes were observed under a microscope.

2.3.3. Cell counting kit-8 (CCK-8) assay. The cell counting kit-8 was applied to determine the cell viability according to the manufacturer's instructions. Around 5×10^3 cells in 100 μL of medium were plated on 96-well plates and cultured for 12 h, 24 h, and 48 h. Cells were divided into six groups: blank control group (cultured with the medium), 25% HA/Col group, 50% HA/Col group, 75% HA/Col group, 100% HA/Col group, and phenol (0.64%) group. After the prescribed incubation period respectively, we add 10 μL of CCK-8 to each well, and cells were further incubated for three hours at 37 °C. Absorbance was measured at the wavelength of 450 nm using Microplate Spectrophotometer (Thermo Fisher Scientific, Waltham, MA, US). All experiments were conducted in triplicate.

2.4. Osteogenesis in vivo

2.4.1. Animal experiments. All animal procedures were performed in accordance with the Guidelines for Care and Use of Laboratory Animals of Guangxi Medical University and approved by the Animal Ethics Committee of Guangxi Medical University.

The male Sprague Dawley (SD) rats (8–9 weeks old, 250–300 g) were used in this research, which was approved by the Animal Welfare Committee of the School of Guangxi Medical University, China. With the help of intraperitoneal injection of pentobarbital (30 mg kg^{-1}), these animals were anesthetized. The mini-incision (1 cm) along the right side of the mandible was made on the skin, followed by periosteotomy and the dissection of the masseter muscle. The critical size defect ($3 \times 3 \times 3$ mm) was created with a dental high-speed turbine handpiece, which cooled continuously with 0.9% saline solution. The mandibular critical-sized defects ($n = 30$) were randomly divided into two groups that received the following implantation materials respectively:

The control group was left empty without any scaffolds.

Collagen scaffolds cooperated with 0.1 mg/100 g rhBMP-2 were implanted into the defects in the experimental group.

SD rats from each group were killed at 1, 4, and 8 weeks after the operation.

2.4.2. Histological evaluation. For histological evaluation, the samples together with surrounding tissues from the original defect area were fixed with 10% formalin for 24 h, then decalcified in 10% the EDTA for ten weeks. Samples were embedded in paraffin, then the serial sections with 5–7 μm thickness were made. Tissue blocks were stained with hematoxylin and eosin (H&E) or stained with Masson trichrome. Eight weeks after the initial implantation of collagen scaffolds cooperated with rhBMP-2, the vital organs, including heart, liver, spleen, lung, and kidney, were harvested and stained with hematoxylin and eosin (H&E) to assay composites-induced toxicity. A light microscope (Carl Zeiss, Jena, Germany) was used to observe the stained slides at ×200 magnifications.

2.5. Statistical analysis

All data analysis was performed using SPSS 13.0 software. One-way ANOVA was used to analyze the differences among the groups, and the statistically significant values were adopted as $p < 0.05$.

3. Results

3.1. Characterization of materials

As shown in Fig. 1A, the porosity of HA/Col scaffolds (60/20, 80/20, and 100/20) was 83.35 ± 0.02, 81.05 ± 0.03, and $78.05 \pm 0.04\%$, respectively. The porosity of Col scaffold was $89.17 \pm 0.01\%$. All the fabricated scaffolds were highly porous. The porosity of the Col (100/20) was significantly lower than that of HA/Col (80/20 and 100/20), while no significant differences could be detected in HA/Col scaffolds of different ratios.

After the water full infiltration treatment, the degree of swelling of the Col scaffolds was around the range of 1600%, while that of the HA/Col scaffolds (60/20, 80/20, and 100/20) was in the range of 1300–1500% (Fig. 1B). With the drying time extended to 18 h, the degree of swelling in Col scaffolds was reduced to approximately 600%. Unlike Col, the prepared HA/Col scaffolds (60/20, 80/20, and 100/20) still possessed a high degree of swelling in the range of 656–678%, which meant that HA/Col could effectively weaken the evaporation of water from the inner area of the scaffolds.

Then mechanical properties of the developed scaffolds were assessed by TS and Eb detection. The developed Col had a TS of 1.01 ± 0.03 MPa, which was significantly different from HA/Col of 80/20 (1.17 ± 0.09 MPa) and 100/20 (1.26 ± 0.02) (Fig. 1C). The same trend can be observed in Eb (Fig. 1D). The Eb of Col was significantly higher than that of HA/Col (100/20). TS and Eb, parameters of mechanism, can indicate the flexibility and strength of materials.

The rate of biodegradation also varied between different 3D scaffolds. The fastest degradation index appeared in pure Col scaffolds which were 38.05% (day 1) and 55.69% (day 21). On the other hand, scaffold with different proportions of HA (60/20, 80/20, and 100/20) showed a slower degradation rate. Meanwhile, the 3D scaffold (100/20) exhibited the lowest degradation rate 11.52% (day 1) and 17.76% (day 21) (Fig. 2A).
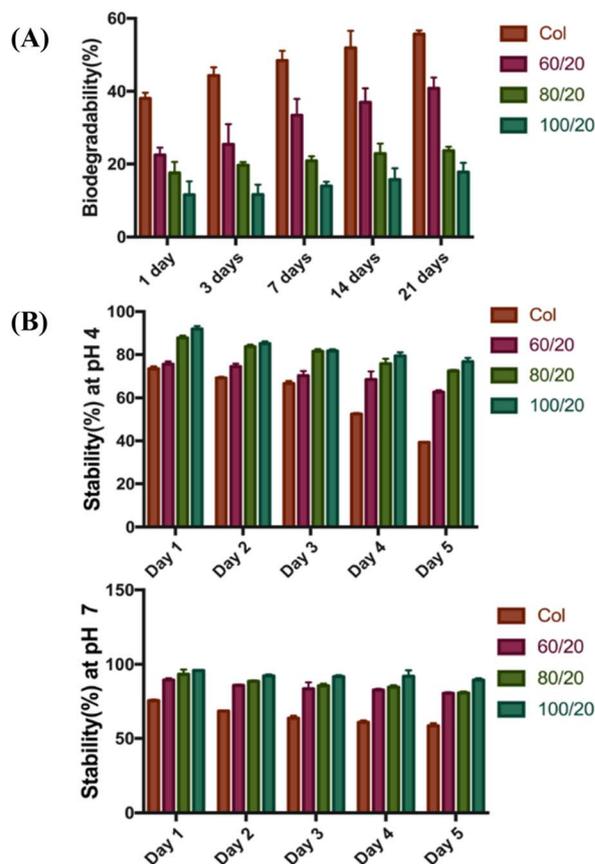

Fig. 2 (A) Enzymatic degradation studies of different scaffolds. (B) Stabilities of scaffolds in aqueous solution: (up) stability test at pH 4.0 and (down) stability test at pH 7.0.

The stability test of 3D scaffolds was shown in Fig. 2B. As the proportion of HA increases, the 3D scaffolds become more stable. In general, scaffolds were more stable in neutral pH (pH 7.0) compared to acidic conditions (pH 4.0). In both cases, the 3D scaffold (100/20) showed the highest stability, while the pure Col scaffolds without HA exhibited the lowest stability.

SEM was applied to study the porous morphologies of HA/Col composites (80/20) and Col scaffold. Fig. 3A1–A3 showed the SEM image of the collagen scaffold, and Fig. 3B1–B3 showed the SEM images of the HA/Col composites. From SEM observations of the Col scaffold, one can see a three-dimensional porous structure, which constituted of a coiled-coil system thrown into a second-order helix. Compared to the relatively smooth-surfaced Col scaffold, HA/Col composites show a rough and porous structure with a large number of nano-HA particulates adhered to the Col surface. The image shows that the aperture of HA/Col was 50–100 μm, and the pores were associated with no clear fixed direction. In conclusion, the micro-scale construction of HA/Col composites shows a porous fibrous collagen matrix embedded with uniformly scattered particles of nano-HA, indicating that nano-HA and Col scaffold were well combined.

FT-IR spectra of nano-HA, Col scaffold, and HA/Col composites (80/20) are shown in Fig. 4. From the spectrum,
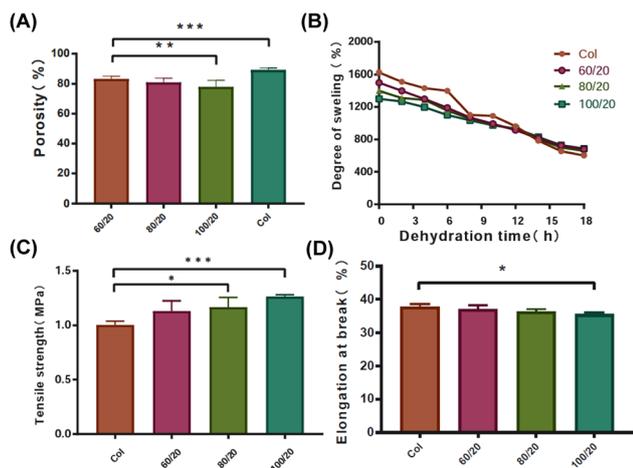

Fig. 1 Physical and mechanical properties of different scaffolds. (A) Porosity. (B) Degree of swelling. (C) Tensile strength, and (D) elongation at break. The data represent mean ± standard deviation with statistically significant differences represented by *$p < 0.05$, **$p < 0.01$, ***$p < 0.001$.
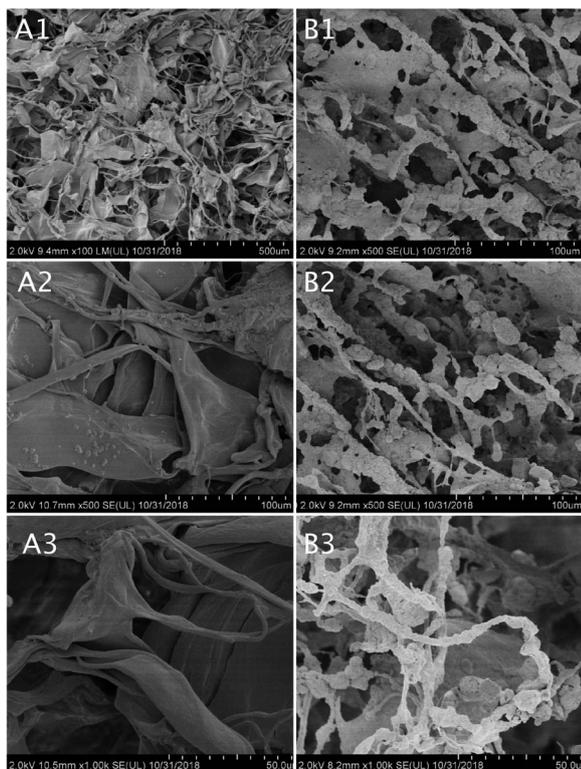
Fig. 3 SEM images of Col scaffold (A) and HA/Col composites (B): (A1 and B1) at 100× magnification, (A2 and B2) at 500× magnification, (A3 and B3) at 1000× magnification.
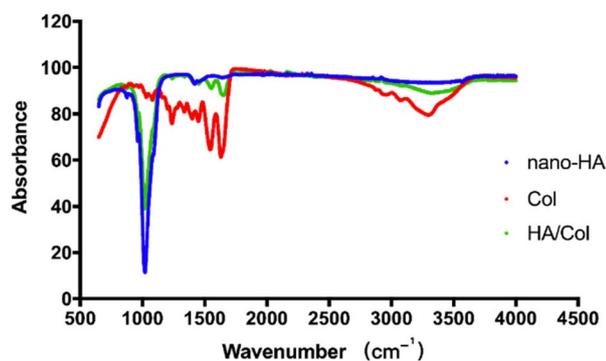

Fig. 4 FT-IR spectrum of nano-HA, Col scaffold, and HA/Col composites.

the typical bands for collagen such as N–H stretching at $\sim$3329 cm^{-1} for the amide A, C–H stretching at $\sim$3076 cm^{-1} for the amide B, C=O stretching at $\sim$1628 cm^{-1} for the amide I, and N–H deformation at $\sim$1543 cm^{-1} for the amide II. The phosphate groups should be considered as HA-related bands. Typically, the phosphate bands are located between 900 and 1200 cm^{-1} in infrared spectra. In the spectrum of HA, the typical stretching vibration bands of phosphoric contours can be observed at 978 and 1023 cm^{-1}. There are also CO_3^{2-} bands located at $\sim$1419 and 1453 cm^{-1}. The characteristic peaks of HA/Col composite can be observed at 978 and 1021 cm^{-1}, corresponding to the peculiar phosphate component. Besides the
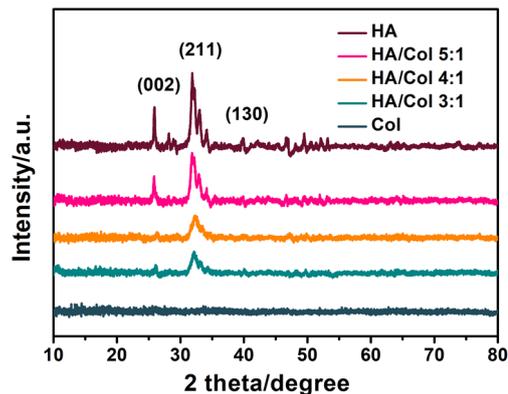

Fig. 5 XRD spectra of nano-HA, Col scaffold, and HA/Col scaffolds with different nHA and Col mass ratios.

typical peaks of phosphate bands in HA, the HA/Col composite also showed characteristic peaks at 1389 and 2982 cm^{-1}, corresponding to the unique carboxyl and methyl group in the Col component, respectively.

HA crystallinity was illustrated by a peak corresponding to (002) at $2\theta = 26°$ and overlapping peaks corresponding to (211) at $2\theta = 32°$. In comparison, the 2θ peak of Col scaffold was wide and dispersed suggesting low crystallinity of pure Col scaffold. In the HA/Col scaffolds groups, the 2θ values were all 20.1° suggesting a crystalline form similar to that of HA. In other words, after adding HA, the crystallinity of the HA/Col scaffold increased compared with pure Col scaffold (Fig. 5).

The TEM micrographs of Col scaffold and HA/Col composites were shown in Fig. 6. At pH 7.3–7.7, the collagen molecules crosslinked to form 60–70 nm D-banded collagen fibrils that aggregated as spindle-shaped fiber
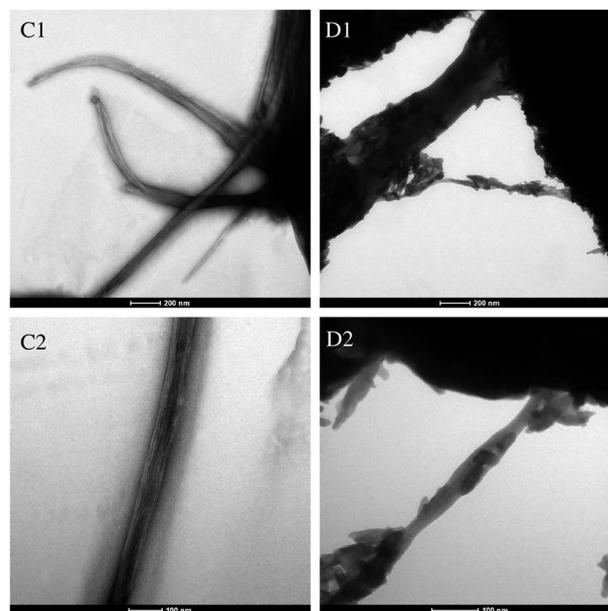

Fig. 6 TEM micrographs of Col scaffold (C1 and C2) and HA/Col composites (D1 and D2). (C1 and D1) at 120 000× magnification, (C2 and D2) at 200 000× magnification.

© 2023 The Author(s). Published by the Royal Society of Chemistry

structures, which differed from typical D-banded collagen fibers (Fig. 6C1 and C2). As to the HA/Col composites, nano-HA crystals formed around the surface of self-assembled collagen fibers, and no crystals got inside the fibers. To sum up, such nanocrystals distribute along collagen fibers with the *c*-axis parallel to the long axis of fibers as observed by TEM (Fig. 6D1 and D2).

3.2. Morphology and CCK8 assay of DPCs

Primary DPCs were inoculated for 24 h and gradually began to adhere. Following 48 h of incubation, a small number of DPCs were deformed and vacuoles-shaped (Fig. 7A–E). Morphology of living cells under the microscope showed that DPCs were long-spindle form and fiber-shaped. After the cocultivation with different concentrations (25%, 50%, 75%, and 100%) of leach liquor, there were no apparent morphological differences between every two groups (Fig. 7A–E). As to the positive control (Fig. 7F), a large number of cells became dissociated and vesiculated form, which means cell death. As Fig. 8 shows, the DPCs incubated with HA/Col leach liquor proliferated with increasing culturing time (from 12 h to 48 h), which was indicated by the OD value of the CCK8 assay. Compared with phenol (0.64%), the OD value was significantly higher in treatment groups after 12 h, 24 h, and 48 h of incubation. From the perspective of trend, there were no visible differences in the cell proliferation between the control group and the groups with leach liquor of different concentrations (25%, 50%, 75%, and 100%) in general (Fig. 8).

3.3. Histological analysis of bone regeneration

In order to evaluate the function of scaffolds and biologics on bone defect repairing *in vivo*, the HA/Col scaffolds and rhBMP-2
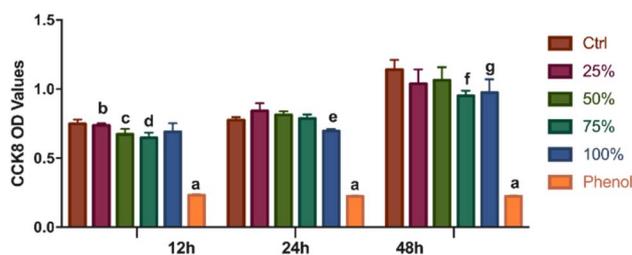

Fig. 8 CCK-8 cell proliferation assay was performed on DPCs treated with leach liquor of different concentrations or phenol (0.64%) on 12 h, 24 h and 48 h. [a] $p < 0.001$ compared with other treatment groups at the same incubation time (12 h, 24 h and 48 h, respectively). [b] $p < 0.01$ compared with 75% group. [c] $p < 0.05$ compared with control group. [d] $p < 0.01$ compared with control group. [e] $p < 0.05$ compared with 50% group. [f] $p < 0.01$ compared with control group. [g] $p < 0.05$ compared with control group.

were implanted in rat mandible bone defects. Histopathological analysis of bone regeneration at different times was performed in H&E (Fig. 9) and Masson trichrome staining sections (Fig. 10). As the H&E staining shows (Fig. 9A), plenty of active osteocytes and fibroblasts are embedded within HA/Col scaffolds. The closer scaffolds get to micro-vessels, the more infiltrated osteocytes and fibroblasts can be observed. At the border of scaffold materials and nature bone tissue, some enlarged hyperchromatic macrophages can be seen (arrows). More newly formed bone tissue could be seen around the implants, and the inflammatory cells were significantly reduced after four weeks (Fig. 9B). After eight weeks, the range of scaffolds has shrunk
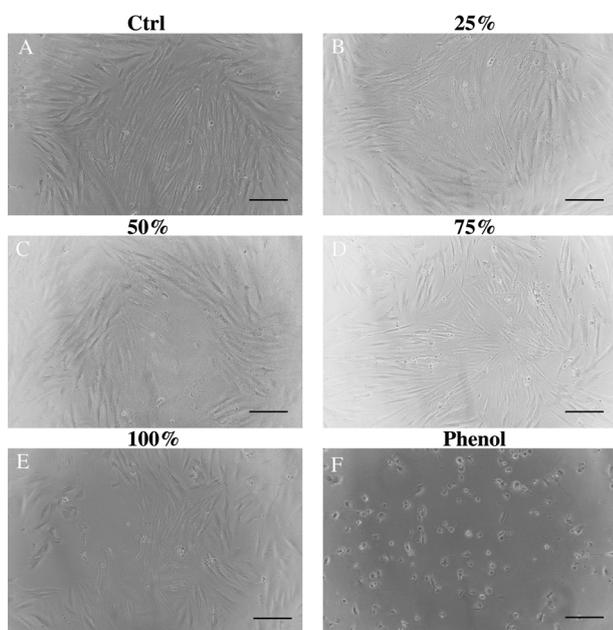

Fig. 7 DPCs morphology was examined under a microscope at 100× magnification after 48 hour incubation. Scale bar, 100 μm.
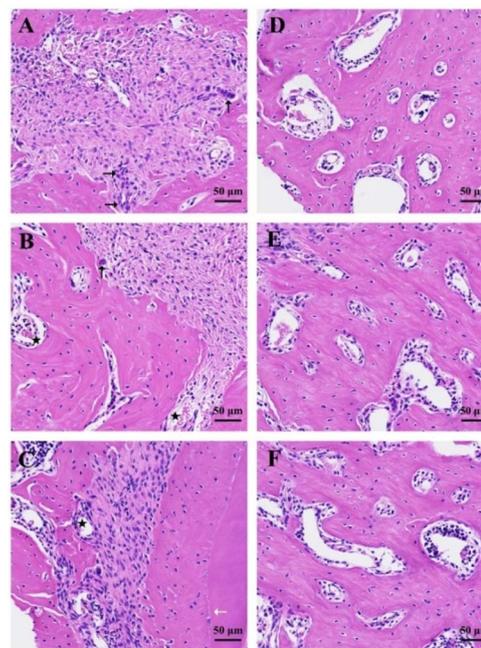

Fig. 9 Histological images of the mandibular bone defect sites by H&E staining at 200× magnification. Experimental group: (A) 1 week, (B) 4 weeks, (C) 8 weeks. Control group: (D) 1 week, (E) 4 weeks, (F) 8 weeks. Arrows: multinucleated macrophages. Star: blood cells.
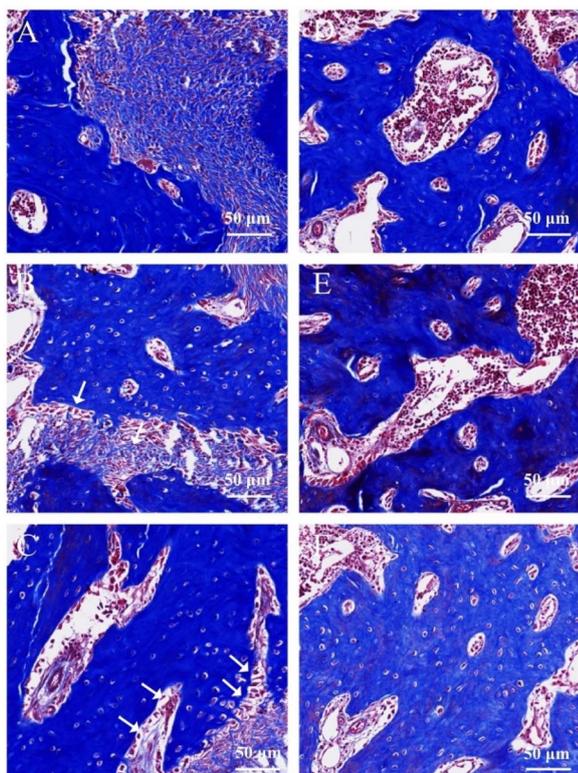
Fig. 10 Masson trichrome staining of the mandibular bone defect sites at 200× magnification. Experimental group: (A) 1 week, (B) 4 weeks, (C) 8 weeks. Control group: (D) 1 week, (E) 4 weeks, (F) 8 weeks. Arrows: osteoblast.

Fig. 11 The histopathological sections of rat major organs, H&E bar 50 μm. Control group: (A) heart, (B) liver, (C) spleen, (D) lung, (E) kidney. Experimental group: (F) heart, (G) liver, (H) spleen, (I) lung, (J) kidney.

further (Fig. 9C). The relatively clear boundary can be seen in osseous tissues at different stages of development (arrows). Little marrow cells could be found in early-formed external bone tissue. A small number of osteocytes can be detected around the residual scaffolds. On the border of scaffolds and original bone tissues, new capillaries have risen significantly (Fig. 9B and C, asterisk). When no materials were implanted in the control group, the defect sites presented with porous and vacant bone cavities.

Masson trichrome staining was also applied to give an accurate assessment of newly formed bone tissues and residual scaffolds. The degree of mineralization influences the effects of staining. Naturally, mature bone tissue can be stained to brick red, immature bone tissue to light blue. One week later, the HA/Col scaffolds were stained light blue, while the surrounding natural bone tissues were hyperchromatic (Fig. 10A). With the prolonging of implant-time, the HA/Col scaffolds were displaced by mature bone tissue. At the edge of residual scaffolds, the regular alignment of simple columnar epithelia could be discovered, which were considered as osteoblast (Fig. 10B, arrows). At 8 weeks after the operation, new bone regenerated and penetrated through the interlinked pores into the center of HA/Col composite materials, as shown in Fig. 10C. The boundary between host bone and HA/Col scaffolds was unclear due to the amount of mature bone tissue that grew into the pores of the materials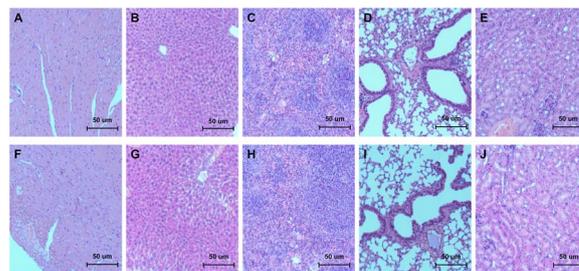. Meanwhile, there was a significant increase in the proliferation of osteoblast (Fig. 10C, arrows). As shown in Fig. 11, the implantation of HA/Col scaffolds and rhBMP-2 did no histopathological damage or problems to the main organs compared to the control group.

4. Discussion

Bone is one kind of natural tissue, which owns a complex hierarchical structure, mainly comprised of hydroxyapatite (HA) (50–70%), an organic matrix composed of type I collagen (20–40%).[10] At the molecular level, collagen molecules assembled, forming anisotropically oriented collagen fibrils, with nano-HA crystals filling the intermediate region located in the individual collagen fibrils. A number of closely packed collagen fibrils arranged in concentric circles called lamellae form the basic unit of the bone macrostructure called the osteon. The HA–Col scaffold of bone can provide an ideal, spongy, porous structure, providing a three-dimensional space for cell nutrient transfer, adhesion, migration, and growth.[25] In addition, the nano-HA particles embedded in the scaffold can improve the surface roughness, thus helping the surface area of the scaffold to promote cell adhesion.[26] In the present work, we synthesized HA/Col scaffold with freeze-dried technology. Traditionally, the first inducing collagen fibrillogenesis was prepared via gelation, followed by freeze-drying to generate porous scaffolds.[25] The pore size and orientation can be controlled by reaction parameters, such as freezing direction, pH of the solution, solute concentration, and freezing rate.[27] The slower pace of cooling and higher pH can create scaffolds with larger pores.[11] Moreover, pore sizes of freeze-dried collagen scaffolds are directly proportional to increasing collagen concentration.[28] Two different fabrication methods have been developed to structure nano-HA/Col scaffolds: (1) before the freeze-drying process, the nano-HA particles were suspended in a collagen slurry. (2) Collagen scaffolds were immersed in a nano-HA suspension after lyophilization. Compared with the immersion method (method 2), nano-HA/Col scaffolds, constructed according to the suspension method, were found to be more stable and stiffer,[29] which was critical to clinical application. So, the first method was adopted in our study.

From previous studies, a biomaterial scaffold with porosity around 80–90% was capable of facilitating the proliferation, implantation, and regular function of fibroblasts and

osteoblasts.[30] Our results indicated that the porosity values of HA/Col (60/20, 80/20, and 100/20) were close to this range, which were sufficiently porous enough to support nutrient diffusion, vascularization, cell penetration, and proliferation throughout the entire scaffold's structure.

The high level of swelling and water retention allows biological scaffolds to absorb the inflammatory exudation in the bone defects and create a moist environment to promote healing. The absorption-swelling experiment showed Col scaffolds possessed a maximum swelling rate. With the increase in the proportion of HA, the swelling ratio of HA/Col (60/20, 80/20, and

100/20) decreased gradually. The result can be related to the relatively tight pore structure of the HA/Col, which reduces the porosity. But, the HA/Col scaffolds showed longer moisture retention time, which can be ascribed to the ability of HA to retain water.[30] With the addition of nano-HA, HA/Col scaffolds showed greater mechanical strength, which can be verified by TS and Eb and is consistent with previous studies.[31] In effect, the high mechanical strength could help to improve the stability of tissue-engineering bone scaffold so as to resist some external mechanical stresses and obtain ideal healing conditions. Considering the balance between mechanical strength and porosity (strength $\propto$ 1/porosity), the HA/Col scaffolds (80/20) were used in our research.

As shown in SEM photographs (Fig. 3), the HA/Col scaffolds were well-developed macropore structures with a pore size of around 50–100 μm after the lyophilization process. Studies suggested that macro-porosity (pores > 50 μm) is deemed sufficient for osteogenesis by ion transport and facilitating cell, and micro-porosity (pores < 20 μm) can promote protein adsorption and increase the attachment points for osteoblasts, improving bone growth into scaffolds.[32] To sum up, the HA/Col scaffolds were structurally ideal for bone tissue engineering.

The analysis in Fig. 6 showed the nano-HA crystals formed around the self-assembled collagen fibers without infiltrating, which could be attributed to the limitation of size exclusion.[33] But the dispersive HA crystals exhibited a shape very similar to that observed in bone tissue, *i.e.*, thin plate-like crystals. The FT-IR absorption spectrum measurement was carried out to investigate the hierarchical relationship between the nano-HA crystals and collagen scaffolds.

Table 1 Assignments of the observed vibrational frequencies of nano-HA, Col scaffold and HA/Col composites

Assignments	Observed vibrational frequencies wavenumber (cm^{-1})		
	Nano-HA	Col	HA/Col
Structural OH	3583	—	—
H_2O adsorbed, N–H	—	3329	3366
C–H	—	3076	—
C–H_3 group	—	2980	2982
H_2O adsorbed, C=O	1683	1628	1664
N–H, C–N	—	1543	1541
CO_3^{2-}, pyrrolidine rings	1453	1451	1455
C–H, CO_3^{2-}	1419	1402	1418
–COO^-	—	1389	1389
C–N, N–H	—	1240	1240
PO_4^{3-} bend	1023	—	1021
PO_4^{3-} stretch	978	—	978

Cross-linked Col scaffolds

HA/Col 3D scaffolds after lyophilization

Wall of pore

Microstructure of Col scaffolds

Microstructure of HA/Col scaffolds

collagenous fiber

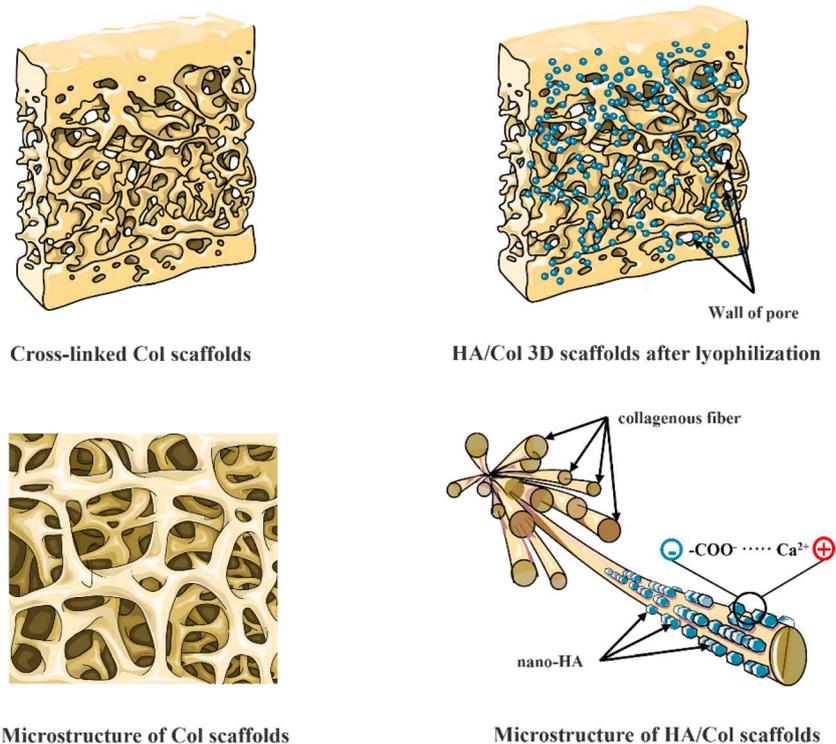⊖ -COO^- ······ Ca^{2+} ⊕

nano-HA

Fig. 12 Schematic of homogeneous 3D HA/Col and Col scaffolds and bonding mechanism.

The observed vibrational frequencies were shown in Table 1. As regards the HA/Col composites preparations, a few papers published so far demonstrated that chemical interaction between HA and Col can be evaluated from the infrared spectrum of HA/Col composite.[11] The FT-IR vibration peak of HA/Col can be observed a shift of the band corresponding to –COO⁻ stretching to lower wavenumber. This phenomenon can be explained as the formation of a new chemical bond between Ca^{2+} ions on the hydroxyapatite surface and –COO⁻ on collagens.[34] However, no alterations can be indicated in the Col vibration mode in this work. So, the combination of nano-HA crystals and collagen scaffolds can be attributed to electrostatic attraction without chemical bonds. These charge storage regions of HA crystals may result from calcium- (positive) and carboxyl- (negative) rich areas of collagen scaffolds. The specific process can be illuminated in Fig. 12.

It can be seen that the amorphous-to-crystalline transformations were witnessed by XRD analyses in Fig. 5. Pure Col scaffold developed no diffraction peaks, however, the $2\theta = 32°$ values of the HA showed XRD diffraction patterns which are consistent with the typical XRD spectra of hydroxyapatite. Collectively, the results demonstrated that the crystalline phase of the HA/Col scaffolds was calcium phosphate.

The biocompatibility of HA/Col composite material *in vitro* and vivo was also investigated. Analysis of co-culture *in vitro* and histopathological examination of vital organs showed the porous scaffold material has the function of less toxic and side effects. Although the histological observation *in vivo* showed a few inflammatory cells infiltration in the area surrounding the residual porous scaffolds in the early implantation samples (1 week and 4 weeks), the infiltrating inflammatory cell decreased significantly with prolonged implant-time. According to the report, early-stage inflammatory cell infiltration owing to the Th1 lymphocytes which produce pro-inflammatory cytokines leading to macrophage activation, can be associated with poor tissue remodeling and rejection of both allo- and xenograft transplants. On the other hand, Th2 lymphocytes produce other cytokines that do not activate macrophages and are probably associated with graft incorporation which leads to the infiltrating inflammatory cell decreased with prolonged implant-time.[4] Thus, HA/Col composite indicated ideal histocompatibility to some extent from a comprehensive perspective.

Though HA/Col scaffolds could offer stable and splendid regeneration conditions, and many composite materials have been developed by researchers for bone tissue engineering with certain ratios of HA and Col, considering their limited osteoinduction ability and the demands of modern tissue engineering, local delivery of growth factors should be supplemented to reinforce complementary advantages.[16] Among those biological mediators, bone morphogenetic proteins (BMPs) play a prominent part in osteogenic differentiation. Numerous *in vitro* and *in vivo* studies have confirmed their potential and safety in inducing osteogenic cell differentiation.[35,36] In the past few years, the application of BMPs, especially BMP-2 has become more critical for the treatment of bone defects and has been approved by the FDA for use in human spinal fusion, oral-maxillofacial applications, and the treatment of certain

fractures.[37] But considering their short half-life, BMPs suffer a significant loss of activity *in vivo*, which is limited by proteolysis.[35] Although the high dosage of BMPs could offset this loss, the potential side effects and high cost adversely affect its clinical potential. In our test, the commercialized rhBMP-2 was coated with soy lecithin and gelatin, to create sustained-release medical systems so that they can be released and trigger or modulate new bone formation, while the porous HA/Col composite scaffolds could induce the cells easily migrate into the porous body and improve osteoconduction and remodeling at the implant site.[16,38] Therefore, it is currently widely recommended that incorporating BMPs into biomaterial scaffolds is effective for the treatment of critical bone defects.

However, many scholars believed that the unfavorable conditions of the reactions and loading might adversely affect the bioactivity of growth factors for some reasons, like the chemical modification of proteins, the denaturing of the protein drugs by organic solvent, and attaching the cleavable linker to the complicated multi-step procedure.[39] Thus, in this study, the rhBMP-2 wasn't loaded to HA/Col composite scaffold but synchronous implantation in this study for avoiding the above weaknesses.

As an active bioceramic material, HA has advantages such as osteoconductivity and transportability of active ions, which are more conducive to close interaction with cells and tissues in the biological environment. However, no matter whether the HA composite combines with inorganic, organic, or multi with organic/inorganic materials, the microstructural surface characteristics, such as grain size, microporosity, surface roughness, and specific surface area, have been firmly proposed as important determinants in osteoinduction. The reported intrinsic osteoinductive characteristics of the materials may be explained by the fact that these factors control their capacity to link with proteins or peptides.[40]

The histological evaluation of HA/Col scaffold and rhBMP-2 implanted in the mandibular defect of SD rats showed that they exhibited high efficiency of bone regeneration by the induction of osteoblastic differentiation and angiogenesis. On the one hand, it could be interpreted as the multiple roles of rhBMP-2 in bone reconstruction, from the migration of mesenchymal stem cells to differentiation into osteoblasts during both early and late periods of time.[37] On the other hand, BMP-2 could accelerate angiogenesis by activating MEK/ERK, PI3K/Akt, and Id-1/integrin α6 signaling pathway.[41] So, with the help of the cooperation between HA/Col scaffolds and BMP-2, the regeneration of large-scale bone defects may actually become possible.

5. Conclusions

In this study, we developed a biological 3D HA/Col scaffold by optimized freeze-drying technology. This scaffold showed porous properties, a high level of swelling, and relatively ideal mechanical properties, owing to its unique hierarchical structure and ingredients. Analysis of co-culture *in vitro* showed the excellent biocompatibility of HA/Col scaffolds. Histological evaluation *in vivo* confirmed that the HA/Col scaffolds could engineer an ideal environment for osteoblast transfer,

adhesion, migration, and growth. Moreover, the rhBMP-2, a multifunctional cytokine, could further promote osteoblastic differentiation and angiogenesis in bone defect areas, exhibiting high efficiency of bone regeneration. Therefore, such an intelligent biological repair system has potential application in regenerative medicine.

Author contributions

Hongyu Xie: investigation, writing. Sijie Ruan: investigation, data curation, funding acquisition. Minlong Zhao, Jindong Long: data curation, writing – review & editing. Xueling Ma, Jinhong Guo: writing – review & editing, validation. Xuandong Lin: conceptualization, supervision, funding acquisition, and project administration.

Conflicts of interest

No potential conflict of interest is reported by the authors.

Acknowledgements

References

1 Y. Kinoshita and H. Maeda, Recent developments of functional scaffolds for craniomaxillofacial bone tissue engineering applications, *Sci. World J.*, 2013, 863157.

2 B. T. Goh, S. Lee, H. Tideman and P. J. Stoelinga, Mandibular reconstruction in adults: a review, *Int. J. Oral Maxillofac. Surg.*, 2008, **37**(7), 597–605.

3 E. Neovius and T. Engstrand, Craniofacial reconstruction with bone and biomaterials: review over the last 11 years, *J. Plast. Reconstr. Aesthetic Surg.*, 2010, **63**(10), 1615–1623.

4 A. Oryan, S. Alidadi, A. Moshiri and N. Maffulli, Bone regenerative medicine: classic options, novel strategies, and future directions, *J. Orthop. Surg. Res.*, 2014, **9**(1), 18–45.

5 B. Yilmaz, A. Z. Alshemary and Z. Evis, Co-doped hydroxyapatites as potential materials for biomedical applications, *Microchem. J.*, 2019, **144**, 443–453.

6 W. G. De Long Jr, T. A. Einhorn, K. Koval, M. McKee, W. Smith, R. Sanders and T. Watson, Bone grafts and bone graft substitutes in orthopaedic trauma surgery. A critical analysis, *J. Bone Jt. Surg., Am. Vol.*, 2007, **89**(3), 649–658.

7 S. Li, W. C. Liu, Y. H. Chang, X. Liu, C. L. Chang, C. Lin and R. J. Chung, Preparation and in vivo investigation of oligomeric proanthocyanidins cross-linked collagen serving as synthesized tissue regeneration membrane, *Mater. Sci. Eng., C*, 2019, **101**, 640–649.

8 A. J. Nathanael, A. Oyane, M. Nakamura, I. Sakamaki, E. Nishida, Y. Kanemoto and H. Miyaji, In Vitro and In Vivo Analysis of Mineralized Collagen-Based Sponges Prepared by a Plasma- and Precursor-Assisted Biomimetic

Process, *ACS Appl. Mater. Interfaces*, 2017, **9**(27), 22185–22194.

9 B. J. Bielajew, J. C. Hu and K. A. Athanasiou, Collagen: quantification, biomechanics, and role of minor subtypes in cartilage, *Nat. Rev. Mater.*, 2020, **5**(10), 730–747.

10 Y. Moriguchi, B. Borde, C. Berlin, C. Wipplinger, S. R. Sloan, S. Kirnaz, B. Pennicooke, R. Navarro-Ramirez, T. Khair, P. Grunert, E. Kim, L. Bonassar and R. Hartl, In vivo annular repair using high-density collagen gel seeded with annulus fibrosus cells, *Acta Biomater.*, 2018, **79**, 230–238.

11 B. Pennicooke, I. Hussain, C. Berlin, S. R. Sloan, B. Borde, Y. Moriguchi, G. Lang, R. Navarro-Ramirez, J. Cheetham, L. J. Bonassar and R. Hartl, Annulus fibrosus repair using high-density collagen gel an in vivo ovine model, *Spine*, 2018, **43**(4), E208–E215.

12 S. Mondal, U. Pal and A. Dey, Natural origin hydroxyapatite scaffold as potential bone tissue engineering *substitute*, *Ceram. Int.*, 2016, **42**(16), 18338–18346.

13 S. Mondal and U. Pal, 3D hydroxyapatite scaffold for bone regeneration and local drug delivery applications, *J. Drug Delivery Sci. Technol.*, 2019, **53**, 101131.

14 T. Kawai, Y. Tanuma, K. Matsui, O. Suzuki, T. Takahashi and S. Kamakura, Clinical safety and efficacy of implantation of octacalcium phosphate collagen composites in tooth extraction sockets and cyst holes, *J. Tissue Eng.*, 2016, **7**, 2041731416670770.

15 Y. Huang, Y. Wang, L. Chen and L. Zhang, Facile construction of mechanically tough collagen fibers reinforced by chitin nanofibers as cell alignment templates, *J. Mater. Chem. B*, 2018, **6**(6), 918–929.

16 A. Tsuchiya, S. Sotome, Y. Asou, M. Kikuchi, Y. Koyama, T. Ogawa, J. Tanaka and K. Shinomiya, Effects of pore size and implant volume of porous hydroxyapatite/collagen (HAp/Col) on bone formation in a rabbit bone defect model, *J. Med. Dent. Sci.*, 2008, **55**(1), 91–99.

17 W. J. King and P. H. Krebsbach, Growth factor delivery: how surface interactions modulate release in vitro and in vivo, *Adv. Drug Delivery Rev.*, 2012, **64**(12), 1239–1256.

18 S. Vanhatupa, M. Ojansivu, R. Autio, M. Juntunen and S. Miettinen, Bone Morphogenetic Protein-2 Induces Donor-Dependent Osteogenic and Adipogenic Differentiation in Human Adipose Stem Cells, *Stem Cells Transl. Med.*, 2015, **4**(12), 1391–1402.

19 Y. K. Wang, X. Yu, D. M. Cohen, M. A. Wozniak, M. T. Yang, L. Gao, J. Eyckmans and C. S. Chen, Bone morphogenetic protein-2-induced signaling and osteogenesis is regulated by cell shape, RhoA/ROCK, and cytoskeletal tension, *Stem Cells Dev.*, 2012, **21**(7), 1176–1186.

20 M. Zhou, X. Yang, S. Li, K. Kapat, K. Guo, F. H. Perera, L. Qian, P. Miranda and Y. Che, Bioinspired channeled, rhBMP-2-coated β-TCP scaffolds with embedded autologous vascular bundles for increased vascularization and osteogenesis of prefabricated tissue-engineered bone, *Mater. Sci. Eng., C*, 2021, **118**, 111389.

21 J. L. Ong, S. M. Shiels, J. Pearson, S. Karajgar, S. Miar, G. Chiou, M. R. Appleford, J. C. Wenke and T. Guda, Spatial Recombinant Human Bone Morphogenetic Protein

2 Delivery from Hydroxyapatite Scaffolds Sustains Bone Regeneration in Rabbit Radius, *Tissue Eng., Part C*, 2022, **28**(7), 363–374.

22 T. Taniyama, T. Masaoka, T. Yamada, X. Wei, H. Yasuda, T. Yoshii, Y. Kozaka, T. Takayama, M. Hirano, A. Okawa and S. Sotome, Repair of osteochondral defects in a rabbit model using a porous hydroxyapatite collagen composite impregnated with bone morphogenetic protein-2, *Artif. Organs*, 2015, **39**(6), 529–535.

23 R. Xu, H. Xia, W. He, Z. Li, J. Zhao, B. Liu, Y. Wang, Q. Lei, Y. Kong, Y. Bai, Z. Yao, R. Yan, H. Li, R. Zhan, S. Yang, G. Luo and J. Wu, Controlled water vapor transmission rate promotes wound-healing via wound re-epithelialization and contraction enhancement, *Sci. Rep.*, 2016, **6**, 24596.

24 D. Liang, Z. Lu, H. Yang, J. Gao and R. Chen, Novel Asymmetric Wettable AgNPs/Chitosan Wound Dressing: In Vitro and In Vivo Evaluation, *ACS Appl. Mater. Interfaces*, 2016, **8**(6), 3958–3968.

25 S. Zeng, L. Liu, Y. Shi, J. Qiu, W. Fang, M. Rong, Z. Guo and W. Gao, Characterization of Silk Fibroin/Chitosan 3D Porous Scaffold and In Vitro Cytology, *PLoS One*, 2015, **10**(6), e0128658.

26 Y. Cai, S. Tong, R. Zhang, T. Zhu and X. Wang, In vitro evaluation of a bone morphogenetic protein2 nanometer hydroxyapatite collagen scaffold for bone regeneration, *Mol. Med. Rep.*, 2018, **17**(4), 5830–5836.

27 C. J. Doillon, C. F. Whyne, S. Brandwein and F. H. Silver, Collagen-based wound dressings: control of the pore structure and morphology, *J. Biomed. Mater. Res.*, 1986, **20**(8), 1219–1228.

28 C. M. Tierney, M. G. Haugh, J. Liedl, F. Mulcahy, B. Hayes and F. J. O'Brien, The effects of collagen concentration and crosslink density on the biological, structural and mechanical properties of collagen-GAG scaffolds for bone tissue engineering, *J. Mech. Behav. Biomed. Mater.*, 2009, **2**(2), 202–209.

29 G. M. Cunniffe, G. R. Dickson, S. Partap, K. T. Stanton and F. J. O'Brien, Development and characterisation of a collagen nano-hydroxyapatite composite scaffold for bone tissue engineering, *J. Mater. Sci.: Mater. Med.*, 2010, **21**(8), 2293–2298.

30 Z. Lin, T. Wu, W. Wang, B. Li, M. Wang, L. Chen, H. Xia and T. Zhang, Biofunctions of antimicrobial peptide-conjugated alginate/hyaluronic acid/collagen wound dressings promote wound healing of a mixed-bacteria-infected wound, *Int. J. Biol. Macromol.*, 2019, **140**, 330–342.

31 R. J. Kane and R. K. Roeder, Effects of hydroxyapatite reinforcement on the architecture and mechanical properties of freeze-dried collagen scaffolds, *J. Mech. Behav. Biomed. Mater.*, 2012, **7**, 41–49.

32 J. R. Woodard, A. J. Hilldore, S. K. Lan, C. J. Park, A. W. Morgan, J. A. Eurell, S. G. Clark, M. B. Wheeler, R. D. Jamison and A. J. Wagoner Johnson, The mechanical properties and osteoconductivity of hydroxyapatite bone scaffolds with multi-scale porosity, *Biomaterials*, 2007, **28**(1), 45–54.

33 X. Lin, F. Xie, X. Ma, Y. Hao, H. Qin and J. Long, Fabrication and characterization of dendrimer-functionalized nano-hydroxyapatite and its application in dentin tubule occlusion, *J. Biomater. Sci., Polym. Ed.*, 2017, **28**(9), 846–863.

34 M. Kikuchi, S. Itoh, S. Ichinose, K. Shinomiya and J. Tanaka, Self-organization mechanism in a bone-like hydroxyapatite/collagen nanocomposite synthesized in vitro and its biological reaction in vivo, *Biomaterials*, 2001, **22**(13), 1705–1711.

35 M. Geiger, R. H. Li and W. Friess, Collagen sponges for bone regeneration with rhBMP-2, *Adv. Drug Delivery Rev.*, 2003, **55**(12), 1613–1629.

36 C. K. Wang, M. L. Ho, G. J. Wang, J. K. Chang, C. H. Chen, Y. C. Fu and H. H. Fu, Controlled-release of rhBMP-2 carriers in the regeneration of osteonecrotic bone, *Biomaterials*, 2009, **30**(25), 4178–4186.

37 A. H. Yao, X. D. Li, L. Xiong, J. H. Zeng, J. Xu and D. P. Wang, Hollow hydroxyapatite microspheres/chitosan composite as a sustained delivery vehicle for rhBMP-2 in the treatment of bone defects, *J. Mater. Sci.: Mater. Med.*, 2015, **26**(1), 5336.

38 M. Kikuchi, S. Itoh, S. Ichinose, K. Shinomiya and J. Tanaka, Selforganization mechanism in a bone-like hydroxyapatite/collagen nanocomposite synthesized in vitro and its biological reaction in vivo, *Biomaterials*, 2001, **22**, 1705–1711.

39 K. H. Bae, L. S. Wang and M. Kurisawa, Injectable biodegradable hydrogels: progress and challenges, *J. Mater. Chem. B*, 2013, **1**(40), 5371–5388.

40 S. Mondal, S. V. Dorozhkin and U. Pal, Recent progress on fabrication and drug delivery applications of nanostructured hydroxyapatite, *Wiley Interdiscip. Rev.: Nanomed. Nanobiotechnol.*, 2018, **10**(4), e1504.

41 W. C. Chen, C. H. Chung, Y. C. Lu, M. H. Wu, P. H. Chou, J. Y. Yen, Y. W. Lai, G. S. Wang, S. C. Liu, J. K. Cheng, Y. J. Wu, H. I. Yeh, L. Y. Wang and S. W. Wang, BMP-2 induces angiogenesis by provoking integrin alpha6 expression in human endothelial progenitor cells, *Biochem. Pharmacol.*, 2018, **150**, 256–266.